Electron Transfer within Charge-Localized Dinitroaromatic Radical Anions

João P. Telo,*,† Stephen F. Nelsen,*,‡ and Yi Zhao*,§

Centro de Química Estrutural, Instituto Superior Técnico, Av. Rovisco Pais, 1049-001 Lisboa, Portugal, Department of Chemistry, University of Wisconsin, 1101 University Avenue, Madison, Wisconsin 53706-1396, and State Key Laboratory of Physical Chemistry of Solid Surfaces and Department of Chemistry, College of Chemistry and Chemical Engineering, Xiamen University, 361005, People's Republic of China

Received: February 25, 2009; Revised Manuscript Received: May 8, 2009

Rate constants for the intramolecular electron-transfer reaction in the 2,7-dinitronaphthalene ($\mathbf{2}^-$), 4,4′-dinitrotolane ($\mathbf{3}^-$), and 2,2′-dimethyl-4,4′-dinitrobiphenyl ($\mathbf{4}^-$) radical anions in several polar aprotic solvents were estimated by simulating their ESR spectra at different temperatures. At 298 K, the rate constants are in the $2.0-8.0 \times 10^9$ s^{-1} range for $\mathbf{2}^-$ and $\mathbf{3}^-$ and in the $0.4-2.6 \times 10^9$ s^{-1} range for $\mathbf{4}^-$. The rate constants of $\mathbf{3}^-$ and $\mathbf{4}^-$, when corrected for changes in the activation energy (taken as the changes in λ, the transition energy of the mixed valence band), correlate with the inverse of the solvent relaxation time, showing that the reaction is controlled by solvent dynamics. Solvent effects are only found for $\mathbf{2}^-$ in benzonitrile (PhCN), the most viscous solvent studied. Calculations of the rate constants using the Kramers-based theory adapted to the adiabatic limit fit the Eyring plots of $\mathbf{2}^-$ in PhCN and of $\mathbf{3}^-$ and $\mathbf{4}^-$ both in MeCN and PhCN rather well.

Introduction

It was already shown in ESR studies by Ward in 1960 that the *meta*-dinitrobenzene (**1**) radical anion generated by alkali metal reduction in ether solvents has its spin mostly localized on one of the nitro groups,[1] and many groups determined rate constants for electron transfer within such systems in the next decade.[2]

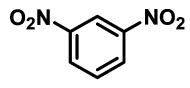

1

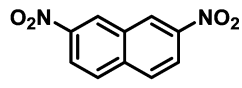

2

These studies predated recognition of the phenomenon of mixed valency, which was developed for metal-centered radical ions in the mid-1960s;[3] therefore, there was no theoretical background for expecting the possibility of charge localization, and the general conclusion of these studies was that solvent and the counterion caused the charge localization that was observed. The simplest mixed valence (MV) compounds have two charge-bearing units **M** (nitro groups in the cases under consideration here) symmetrically attached to a bridge and have an odd oxidation level (−1 in the cases considered here), so that the charges on the **M** groups might be different. When charge is mostly localized so that the charges on the **M** groups are different, the compound is called a Robin−Day Class II MV compound,[3a] and these are the most revealing electron-transfer systems known because Hush theory allows calculation of the thermal electron-transfer rate constant from the optical spectrum.[3c] It was not shown until 2004 that simple UHF/6-31G* calculations, as well as higher level and basis set ones, get charge localization for the 1,3-dinitrobenzene radical anion in the gas phase; therefore, it is predicted to be a Class II MV compound in the absence of either solvent or counterion. CASSCF calculations give a similar result.[4] We reported ESR kinetics for intramolecular electron transfer between the nitro groups of the 2,7-dinitronaphthalene (**2**) radical anion in acetonitrile, benzonitrile, and dimethylformamide (DMF)[2] and pointed out that its optical absorption charge-transfer band in acetonitrile predicted the rate constant observed using Hush theory within the rather wide margin of error for estimation of the electron-transfer distance, d_{ab}, which is necessary to extract the electronic coupling, H_{ab}, and combine with the reorganization energy, λ, which is the transition energy at the band maximum according to the two-state model, to predict the rate constant within an order of magnitude using Marcus−Hush theory,[5] with addition of a quartic term in the diabatic energy surfaces.[6] In this work, we report rate constant measurements on $\mathbf{2}^-$ in two additional solvents, as well as on $\mathbf{3}^-$ and $\mathbf{4}^-$, which lie closer to the borderline between charge localization and delocalization (the Class II, Class III borderline), where simple Hush theory is predicted to have problems because the classical analysis that Hush used leads to cutting off the charge-transfer absorption band at an energy of $\lambda/2$.[7−9] Several dinitroaromatic radical anions that have the Kekule substitution pattern that leads to high H_{ab} values give optical spectra that exhibit vibrational fine structure.[10,11] As pointed out by Heller, observing vibrational fine structure in an absorption spectrum will only occur when vertical excitation gives the excited state near enough to its equilibrium geometry that a wave packet formed on the excited-state surface can return to its origin within about a picosecond.[12] This occurs for Class III (delocalized) compounds, which have the excited-state minimum vertical from the ground-state minimum but has never been observed occur for Class II compounds, for which vertical excitation occurs to a steeply sloping region of their excited-state energy surface, as is clear from Marcus−Hush energy diagrams. We found that the optical spectrum of $\mathbf{3}^-$ has vibrational fine structure that shows it to be charge-delocalized (Class III) in low solvent reorganization energy, λ_s, solvents like hexamethylphosphoramide (HMPA,

* To whom correspondence should be addressed. E-mail: jptelo@ist.utl.pt (J.P.T.); nelsen@chem.wisc.edu (S.F.N.); yizhao@xmu.edu.cn (Y.Z.).
† Instituto Superior Técnico.
‡ University of Wisconsin.
§ Xiamen University.

10.1021/jp9017508 CCC: $40.75
Published on Web 06/08/2009

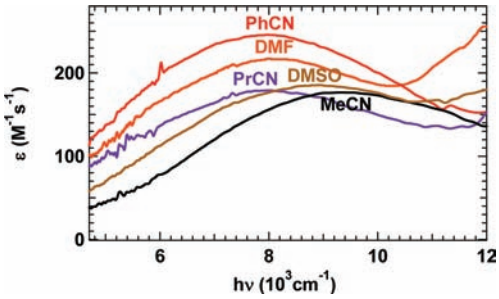

Figure 1. Plots comparing optical absorption spectra of $\mathbf{2}^{\bullet-}$

$(Me_2N)_3PO$) and tetrahydrofuran,[13] and it is shown here that $\mathbf{4}^-$ solutions also contain some delocalized material in HMPA.[14]

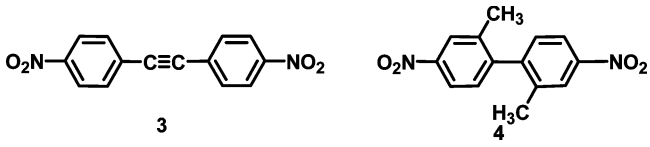

Experimental Section

Commercial 2,7-dinitronaphthalene (**2**) was purified as previously described.[2] 4,4′-Dinitrotolane (**3**)[15] and 2,2′dimethyl-4,4′-dinitrobiphenyl (**4**)[14] were prepared according to known procedures.

The radical anions were prepared in vacuum-sealed glass cells equipped with an ESR tube and a quartz optical cell. Reduction was achieved by contact with a 0.2% Na−Hg amalgam. The nitro compound, an excess of commercial cryptand[2.2.2], used to sequester the sodium counterion, and the Na−Hg amalgam were introduced into different chambers of the cell under nitrogen. The cryptand was degassed by melting under high vacuum before addition of the solvent. The concentration of the samples was determined spectrophotometrically before reduction.

The rate constants for the intramolecular ET reaction were obtained by simulating the experimental ESR spectra. The simulation program solves the Bloch equations for a two-stage model. Asymmetric linebroadening was included in the simulations by making the intrinsic line width Γ of each line dependent on its nitrogen quantum number $\bar{m}$, according to the equation $\Gamma(\bar{m}) = A + B\bar{m} + C\bar{m}^2$.[16]

Results and Discussion

Optical and ESR Spectra. Figure 1 compares the plots of the extinction coefficient versus optical absorption energy for the mixed valence charge-transfer band of $\mathbf{2}^-$ in the five solvents now studied. The electronic couplings extracted from the optical data using a d_{ab} value of 6.44 Å were 310−320 cm^{-1} in MeCN and PrCN and 290−300 cm^{-1} in DMF,[2] which are within experimental error of being the same. The d_{ab} estimate and hence the electronic couplings are only approximate, but there is no evidence that they change with solvent, and we will estimate them at 300 cm^{-1} and use $\lambda = \bar{\nu}_{MV}$, where $\bar{\nu}_{MV}$ is the transition energy at the band maximum for the mixed valence charge-transfer absorption in considering the solvent effect on the rate constant for intramolecular electron transfer.

ESR rate constant and optical data for $\mathbf{2}^-$ in all five solvents now studied, including dimethyl sulfoxide (DMSO) and benzonitrile (PhCN), are summarized in Table 1. The ESR data in DMSO could only be taken over a small temperature range because of its high melting point and compound decomposition at higher temperatures, but although the statistical error is rather high, the slope of the Eyring plot is about that expected from the other solvents; therefore, the short extrapolation to 298 K probably produces a reasonable rate constant. Inclusion of the higher viscosity solvent PhCN makes it clear that electron transfer within $\mathbf{2}^-$ is on the edge of revealing effects of solvent tumbling (see Results and Discussion). A weak spectrum of $\mathbf{2}^-$ was obtained in the especially low λ_s solvent HMPA that showed a broad enough band to represent localized material, with a maximum of about 5800 cm^{-1}, indicating that a detectable amount of Class III material is not present in HMPA for this compound.

The optical spectra for the 4,4-dinitrotolane radical ion ($\mathbf{3}^-$) in five solvents in which it is charge-localized and three in which it is mostly charge-delocalized were previously published (ref 13, Figure 2). Fits to the ESR spectra in acetonitrile at two temperatures are shown in Figure 2.

Table 2 compares the ESR kinetic data with the optical data for $\mathbf{3}^-$ and includes the same information derived from the optical spectrum as Table 1. Although H_{ab} values of about

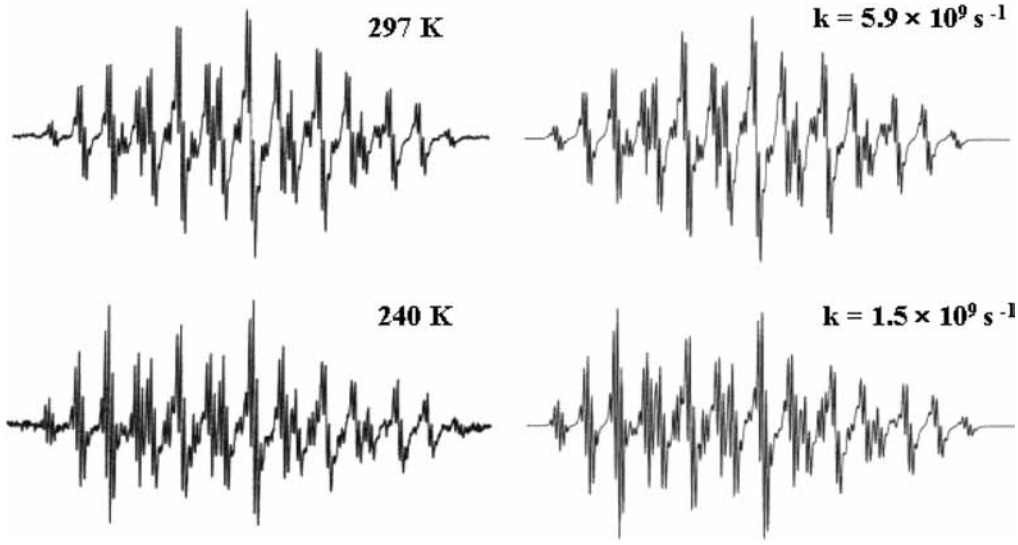

Figure 2. Experimental (left) and calculated (right) ESR spectra for 4,4′-dinitrotolane radical anion ($\mathbf{3}^-$) in MeCN. See the Supporting Information for the simulation parameters.

TABLE 1: Summary of Rate Data for 2^-

quantity	MeCN	PrCN	DMF	DMSO	PhCN
T range, K	225−320	230−305	220−325	291−330	260−300
$\Delta H^{\ddagger}$ kcal/mol	4.4 ± 0.2	3.4 ± 0.5	3.1 ± 0.3	3.3 ± 2.2	4.4 ± 0.8
$\Delta S^{\ddagger}$ cal/mol−deg	0.06 ± 0.9	−2.4 ± 1.7	−2.9 ± 1.0	−2.9 ± 7.1	−0.7 ± 2.9
k(298), 10^9 s^{-1}	3.6 ± 0.3	6.2 ± 0.8	8.0 ± 0.7	5.8 ± 3.4	2.8 ± 0.3
observed k_{rel}	[≡1]	1.7	2.2	1.6	0.7
$\bar{\nu}_{MV}$ cm^{-1}	9360	8040	8100	8930	8000
ΔG^* cm^{-1} [a]	2049	1721	1736	1943	1711
k_{rel} (exp term)	[≡1]	4.9	4.5	1.7	5.1
k_{rel} ratio[b]	[≡1]	2.9	2.0	1.1	7.3
$\langle\tau(295)\rangle$, 10^{-12} s	0.26		0.91	2.0	5.1

[a] $(\lambda/4 - H_{ab} + H_{ab}^2/\lambda)$ using $\bar{\nu}_{MV} = \lambda$ and $H_{ab} = 300$ cm^{-1} (the Hush-derived value). [b] [k_{rel} (exp term)/observed k_{rel}].

TABLE 2: Summary of ESR Rate and Optical Data for 3^-

quantity	MeCN	CH_2Cl_2	DMF	DMSO	PhCN
T range	230−297	210−295	220−295		250−292
$\Delta H^{\ddagger}$	2.7(±0.4)	2.75(±0.21)	3.3(±0.45)		4.7(±0.37)
$\Delta S^{\ddagger}$	−5.0(±1.7)	−6.1(±0.8)	−2.4(±1.8)		+0.6(±1.4)
k(298), $10^9 s^{-1}$	5.6(±0.8)	2.0(±0.2)	7.4(±1.2)	2.7 ± 0.7	3.2(±0.3)
obs. k_{rel}	[≡1]	0.34	1.2	0.48	0.57
$\bar{\nu}_{MV}$ cm^{-1}	11300	10800	9560	10400	9230
ΔG^* cm^{-1} [a] using (H_{ab} value)	241(4000)	181	64	138	41
	621(3000)	533	331	465	283
	1179(2000)	1070	808	885	741
	1914(1000)	1793	1495	1696	1416
k_{rel} (exp term) using (H_{ab} value)	[≡1](4000)	1.33	2.35	1.64	2.63
	[≡1](3000)	1.53	4.06	2.12	5.14
	[≡1](2000)	1.69	5.98	2.56	8.29
	[≡1](1000)	1.79	7.56	2.86	11.05
k_{rel} ratio[b] using (H_{ab} value)	[≡1](4000)	3.9	2.0	3.4	4.6
	[≡1](3000)	4.5	3.4	4.2	9.0
	[≡1](2000)	5.0	5.0	5.3	14.5
	[≡1](1000)	5.3	6.3	6.0	19.4
$\langle\tau(295)\rangle$, 10^{-12} s	0.26	0.56	0.91	2.0	5.1

[a] $(\lambda/4 - H_{ab} + H_{ab}^2/\lambda)$ using $\bar{\nu}_{MV} = \lambda$ and the H_{ab} values stated in the second column. [b] [k_{rel} (exp term)/observed k_{rel}].

750−935 cm^{-1} were obtained in various solvents using the Hush method, $\mathbf{3}^-$ must have a significantly larger H_{ab} value than this because charge delocalization occurs in the low λ_s solvents THF and HMPA. For HMPA, a correlation of $\bar{\nu}_{MV}$ with solvent parameters predicted a value of about 8000 cm^{-1}, implying that H_{ab} is actually larger, on the order of 4000 cm^{-1}.[13] As for the 1,3-dimethoxyphenyl-centered,[17] the R_2N-centered,[18] and the arylhydrazine-centered radical cations,[19] replacing the −C≡C− central bridging unit of tolane-bridged radical anion $\mathbf{3}^-$ by the −CH=CH− unit of the stilbene bridge leads to an increase in rate constant for intramolecular electron transfer, although the effect is smaller in our radical anions than that in the radical cations quoted above. Unfortunately, the rate constant for the stilbene-bridged radical anion is slightly too large for accurate measurement, even in acetonitrile (the 250 K spectrum for the stilbene-bridged compound was fit well using a rate constant of 5×10^9 s^{-1}, but this is at the border of the fast ET limit for this compound, which has a somewhat smaller a_N, 3.2 Gauss, than does $\mathbf{3}^-$, 3.45 at 250 K). Electron transfer is on the order of 2.5 times faster for the stilbene-bridged compound than that for the tolane-bridged one, despite the greater electronegativity of the sp-hybridized carbons of the tolane bridge, which should increase the electronic coupling for the radical anion relative to that of the radical cation.[20] The electronic coupling estimated by Hush's method is, in fact, larger for the tolane-bridged dinitro radical anion than that for the stilbene-bridged one, although the reorganization energy is smaller in each solvent.[13]

The optical spectrum of the 4,4′-dinitro-2,2′-dimethylbiphenyl radical anion ($\mathbf{4}^-$) shows the charge-localized behavior in all

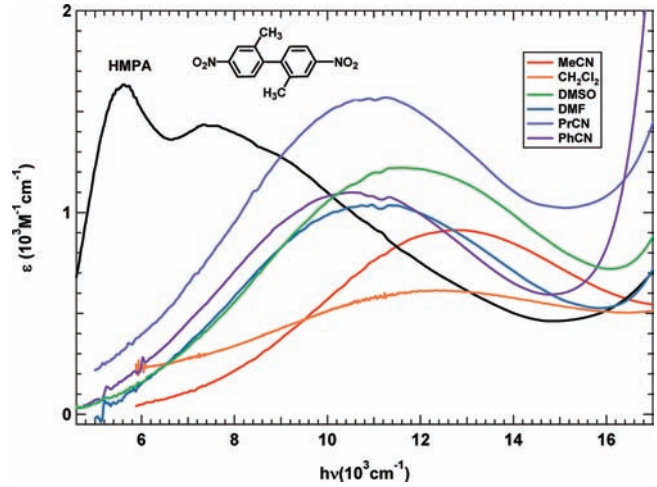

Figure 3. Optical spectra for $\mathbf{4}^-$ in HMPA, where it is charge-delocalized and shows some vibrational fine structure, and that in six solvents where it is charge-localized.

solvents studied except in HMPA, where it shows intermediate behavior in which charge-delocalized features may be clearly seen. In THF, the radical anion precipitates, and in CH_2Cl_2, although both EPR and optical spectra were obtained and are included below, both spectra are considerably less stable than in other solvents. Figure 3 shows the optical spectra of 2,2′-dimethyl-4,4′-dinitrobiphenyl ($\mathbf{4}^-$) in several solvents, including HMPA, where, although the spectrum is rather broad, the first two maxima are attributed to the presence of delocalized

TABLE 3: Summary of ESR Rate and Optical Data for 4^-

quantity	MeCN	CH_2Cl_2	PrCN	DMF	DMSO	PhCN
T range	240−320	240−300	210−300	230−310	*297−330*	260−320
$\Delta H^{\ddagger}$	2.1 ± 0.3	1.0 ± 0.2	2.2 ± 0.4	3.3 ± 0.4	*3.2 ± 0.9*	3.8 ± 0.5
$\Delta S^{\ddagger}$	−11.4 ± 1.2	−15.7 ± 0.8	−9.6 ± 1.4	−4.0 ± 1.6	*−6.2 ± 3.2*	−5.2 ± 1.8
$k(298)$, 10^9 s^{-1}	0.57	0.40	1.26	2.62	*1.28*	0.69
obs. k_{rel}	[≡1]	0.70	2.21	4.60	*2.24*	1.21
$\bar{\nu}_{MV}$ cm^{-1}	12 800	12 300	10 900	11 000	11 600	10 500
ΔG^* cm^{-1} [a] (using H_{ab} value)	2278(1000)	2156	1817	1841	1986	1730
	1513(2000)	1400	1092	1114	1245	1015
	903(3000)	806	550	568	676	489
	450(4000)	376	193	205	279	153
	176(4900)	127	28	33	70	13
k_{rel}(exp term) using (H_{ab} value)	[≡1](1000)	1.81	9.28	8.26	4.09	14.11
	[≡1](2000)	1.72	7.62	6.59	3.60	11.07
	[≡1](3000)	1.59	5.48	5.48	3.00	7.39
	[≡1](4000)	1.43	3.46	3.27	2.28	4.20
k_{rel} ratio[b] using (H_{ab} value)	[≡1](1000)	2.57	4.20	1.79	1.83	11.66
	[≡1](2000)	2.46	3.45	1.49	1.63	9.15
	[≡1](3000)	2.28	2.48	1.10	1.34	6.10
	[≡1](4000)	2.04	1.57	0.71	1.02	3.47
$\langle\tau(295)\rangle$, 10^{-12} s	0.26			0.91	2.0	5.1

[a] $(\lambda/4 - H_{ab} + H_{ab}^2/\lambda)$ using $\bar{\nu}_{MV} = \lambda$ and the H_{ab} values stated in the second column. [b] [k_{rel} (exp term)/observed k_{rel}].

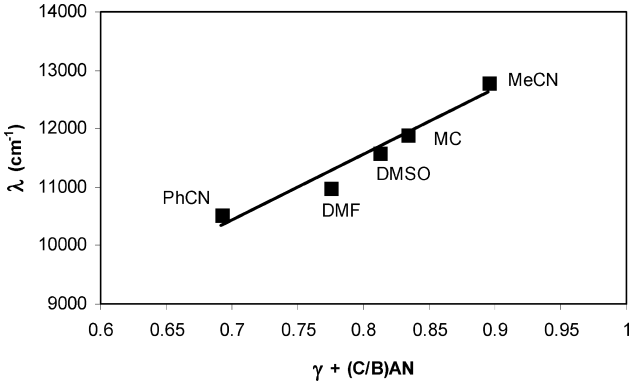

Figure 4. Plot of λ (cm^{-1}) = 2610 + 11190γ + 217AN versus γ + 0.0194AN (r = 0.975) for 4^-.

material, and Table 3 shows the same data for 4^- as Tables 1 and 2 for 2^- and 3^-. H_{ab} values for 4^- of 570 (for PhCN) to 760 cm^{-1} (for PrCN) were obtained using Hush's method, but H_{ab} is clearly higher than this because delocalized material is apparent in HMPA. Using solvent parameters as in our previous work on 3^-,[13] reasonable linearity is seen for a plot of $\bar{\nu}_{MV}$ (taken to be an experimental measure of λ) = $A + B\gamma + C$AN, where γ is the Pekar factor, calculated from the refractive index (n) and static dielectric constant (ε_S) of the solvent as $n^{-2} - \varepsilon_S^{-1}$, and AN is the Gutmann acceptor number of the solvent,[21] as shown in Figure 4. For HMPA (AN = 10.6), this plot predicts λ = 9800 cm^{-1}, suggesting that H_{ab} is on the order of half of this number because delocalized features can be observed, or 4900 cm^{-1}.

Some ESR fits for 4^- are shown in Figure 5. The major problem with the EPR simulations was pseudoequivalence of the H_3 and H_5 splitting constants and those of H_6 and CH_3. Only one constant can be measured for each, but the values are probably slightly different. We adjusted the difference using the appearance of the 3,5,3′,5′ quintet intensities, which deviate from the usual 1:4:6:4:1 (difference of 0.1 G used for all spectra). No similar adjustment appeared necessary in the H_6 and CH_3 cases. Another problem was the choice of the splitting constants for the nearly neutral nitroaromatic group. Using 0 for all does not reproduce the broadening of both the N quintet and the 3,5,3′,5′ H's quintet, which occurs simultaneously at the lowest temperatures. Using 0 for the H's (3′ and 5′) and 0.1 for N does produces good fit for most solvents, but for MeCN, better fit was obtained using a_H = 0 and a_N = 0.35 G. These values were used in all temperatures. Contrary to 4^-, the 4,4′-dinitrobiphenyl radical anion and its 3,3′-dimethyl derivative show EPR spectra in the fast region with no broadening due to dynamic effects. The fact that 4^- has the biggest angle of torsion between aromatic rings decreases the electronic coupling enough to slow the rate to measurable sizes.[14] The same effect was found in biphenyl-bridged bis(hydrazine) radical cations. While the biphenyl-4,4′-diyl radical cation had a rate constant of 1−2 × 10^8 s^{-1} in MeCN, the intramolecular ET reaction in its 2,2′,6,6′-tetramethyl derivative was too slow to be detected by EPR, and no Class II band was visible in the optical spectrum.[22]

Comparison of Kinetic Data on 2^-−4^-. We show the rate constants relative to 2^- in MeCN for all three compounds in Table 4.

The pattern is complex, partially because λ_s is different in different solvents, which directly affects the barriers for electron transfer, but also because the pre-exponential factor is changing with solvent. Because the relationship between rate constants and energies is exponential and the reorganization energies are different for each solvent, we convert these rate ratios to changes in $\Delta G^{\ddagger}$ (kcal/mol) using $\Delta\Delta G_{cor} = \ln(k/k_{2^-,MeCN}) + [(\bar{\nu}_{MV}(\text{solvent}) - \bar{\nu}_{MV}(\text{MeCN})]/4 \times 349.8)$ for each compound that is corrected for the effect of the changes in λ because the point where the free-energy surfaces cross in Marcus theory is $\lambda/4$ and there are 349.8 cm^{-1} per kcal/mol. Because especially 3^- and 4^- lie close to the Class II/III borderline, they must have quite small barriers, and we expect to see effects of "solvent friction" on the pre-exponential factor, which at the limit of a very small barrier is supposed to make it become proportional to $1/\tau$, where τ is the lifetime for solvent tumbling. The best experimental measures of average τ appear to arise from the resolvation of coumarin 153 experiments carried out by Maroncelli and co-workers,[23] which are available at 295 K and are included at the bottom of Tables 1−3 for each available solvent. Butyronitrile unfortunately was not studied. In Figure 6, we plot $\Delta\Delta G_{cor}$ versus $1/\tau(295)$ for the three compounds discussed here. There is a lot of scatter in these plots, as would be expected because the importance of solvent tumbling in

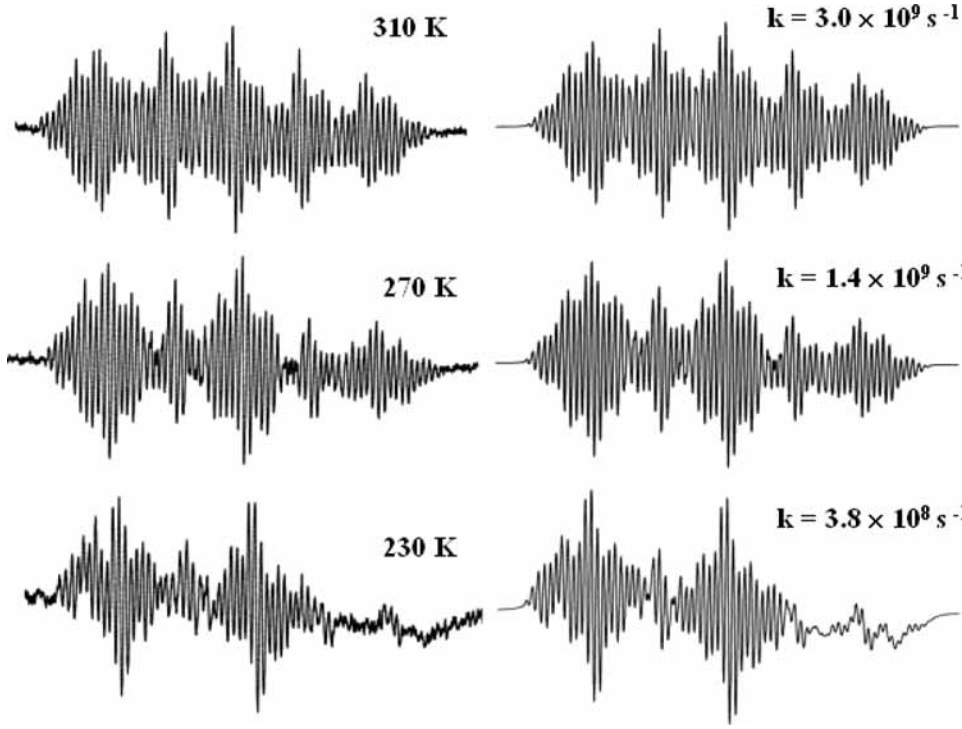

Figure 5. ESR spectra (left-hand side) and corresponding simulations (right-hand side) of the 4,4′-dinitro-2,2′-dimethylbiphenyl radical anion ($\mathbf{4}^-$) in DMF at three temperatures. See the Supporting Information for the simulation parameters.

TABLE 4: Comparison of k_{rel} 298 Values (all relative to $\mathbf{2}^-$ in MeCN)

cmpd	MeCN	CH_2Cl_2	PrCN	DMF	DMSO	PhCN
$\mathbf{2}^-$	≡1.0		1.7	2.2	∼1.6	0.8
$\mathbf{3}^-$	1.6	0.6		2.1	∼0.8	0.9
$\mathbf{4}^-$	0.16	0.11	0.35	0.72	*∼0.36*	0.19

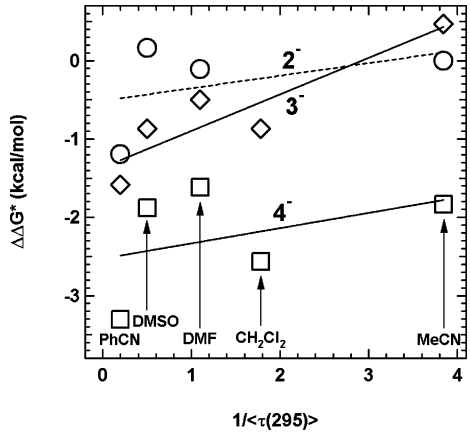

Figure 6. Plots of $\Delta\Delta G^{\ddagger}$ versus $1/\langle\tau(295)\rangle$ for $\mathbf{2}^-$ (circles), dotted regression line, $\mathbf{3}^-$ (diamonds), and $\mathbf{4}^-$ (squares).

affecting the pre-exponential factor will vary as changing solvent changes λ_s. Nevertheless, these compounds show the trend toward lower $\Delta\Delta G_{cor}$ as $1/\langle\tau(295)\rangle$ decreases, which is expected for solvent friction affecting the pre-exponential factor. The slopes are in the order of $\mathbf{3}^- > \mathbf{4}^- > \mathbf{2}^-$. This is rather clearly the order of how close these compounds lie to their II/III borders, from the optical spectra observed for these compounds in HMPA, which is the lowest λ_s solvent that we have found for these radical anions. In HMPA, $\mathbf{3}^-$ shows very predominately the delocalized material spectrum (ref 13, Figure 2), while $\mathbf{4}^-$ shows easily detectable delocalized material, but the majority of the spectrum is caused by the much broader and lower ε localized material spectrum (see Figure 3), and $\mathbf{2}^-$ does not show appreciable amounts of the delocalized material spectrum in HMPA. We also note that for $\mathbf{2}^-$, only the rate constant in PhCN, the most viscous and lowest λ_s solvent studied, appears to be appreciably affected by solvent tumbling.

TABLE 5: Parameters Used for Figures 7−9

	$\mathbf{2}^-$	$\mathbf{3}^-$		$\mathbf{4}^-$	
		solvent			
	PhCN	MeCN	PhCN	MeCN	PhCN
$\bar{\nu}_{MV} = \lambda_s + \lambda_v$	8000	11300	9230	12800	10500
λ_v, cm^{-1}	3760	3070[a]	3070[a]	5300[b]	5300[b]
H_{ab}, cm^{-1}	480−250	2200	2500	3150	4900
ω_o, cm^{-1} [a]	200−600	(1000)	(1000)	(1000)	(1000)
ln b[c]	−32.1	−30.0	−31.7	−27.4	−30.84
H kJ/mol[c]	11.6	1	11.6	1	11.6

[a] Using the size calculated (B3LYP/6-31G*) for 4-nitrotolane. [b] Using the size calculated (B3LYP/6-31G*) for 2,2′-dimethyl-4-nitrobiphenyl. [c] The temperature dependence of τ was approximated as τ (s) = b exp(H/RT).

Kramers-like Theory Fits to the Kinetics for $\mathbf{3}^-$ and $\mathbf{4}^-$. Zhao and co-workers have recently proposed a quantum Kramers-like theory to electron-transfer rate constants in the crossover region between the nonadiabatic and adiabatic limits.[24] The quantum Kramers-like theory is based on the Kramers theory for the calculation of the adiabatic chemical reaction rate constants in solvent but incorporate the nonadiabatic transition probability. [25,26] The numerical simulations for a model system have demonstrated that it correctly predicts the results from the Fermi golden rule in weak electronic coupling and the Kramers theory in the strong electronic coupling.[15] We consider the fits obtained by this approach here. The parameters used for these fits are shown in Table 5. The $\bar{\nu}_{MV}$ value was used as λ, and the values of λ'_v calculated using B3LYP/6-31G* were used to estimate λ_s. In great contrast to using Golden Rule theory, with the large H_{ab} values used, the rate constant is essentially

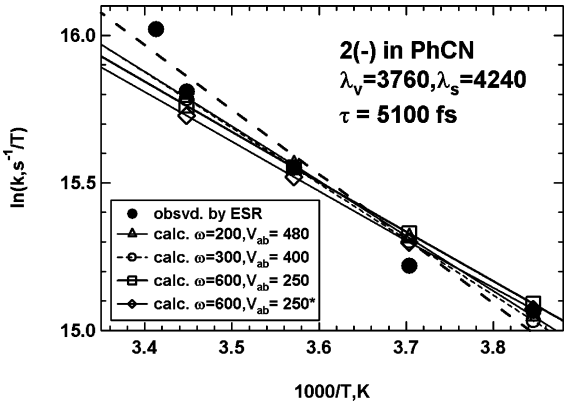

Figure 7. Fits obtained for $\mathbf{2}^-$ in benzonitrile. The calculation marked with a * is for the ln*b* and *H* values shown in Table 5.

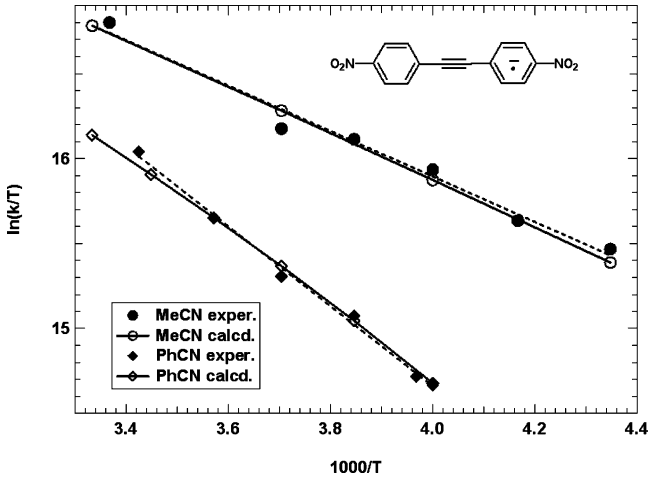

Figure 8. Fits to ESR rate constants for $\mathbf{3}^-$ in MeCN and PhCN (solid circles) using Kramers-like theory with the parameters of Table 5.

independent of ω_o; a value of 1000 cm^{-1} was employed, but the same result was obtained with $\omega_o = 2000$ cm^{-1}. We used eq 1 for the temperature dependence of τ in this work[27]

$$\ln \tau = \ln b + H/RT \quad (1)$$

with the *H* values recommended by Grampp and Jaenicke (1 kJ mol^{-1} for MeCN and 11.6 kJ mol^{-1} for PhCN), and adjusted ln *b* to fit the slopes of the Eyring plot lines using the H_{ab} values for MeCN and PhCN, shown in Table 5. The ln *b* values reported by Grampp and Jaenicke were −29.6 for MeCN and −32.1 for PhCN.

Figures 7−9 show fits obtained for $\mathbf{2}^-$, $\mathbf{3}^-$, and $\mathbf{4}^-$, respectively. The data for $\mathbf{2}^-$ in Figure 7 use Kramers-like theory. As pointed out previously,[2] the rate constants for $\mathbf{2}^-$ are not principally controlled by solvent tumbling, and although all of the calculations gave smaller slopes than the experimental data (which produce a noticeable curve in benzonitrile), comparable temperature dependence was calculated using a variable τ and a constant one of 5100 fs. Very similar temperature dependence was found using ω_o values in the range of 200−600 cm^{-1} when V_{ab} was in the range of 480−250 cm^{-1}, but the slope was noticeably less and, hence, farther from the experimental data using $\omega_o = 1000$ cm^{-1} with $V_{ab} = 150$ cm^{-1}. We previously estimated V_{ab} for $\mathbf{2}^-$ at about 180 cm^{-1} in PhCN from its optical spectrum using a calculated d_{ab} value of 6.44 Å,[2] but it is not obvious what would be the best d_{ab} value to use. The data for $\mathbf{3}^-$ and $\mathbf{4}^-$ in Figure 8 and 9 both indicate rate constants that

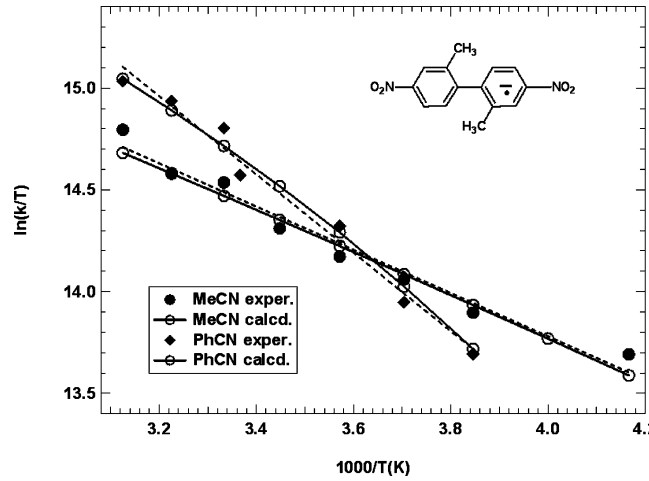

Figure 9. Fits to ESR rate constants for $\mathbf{4}^-$ in MeCN and PhCN (solid circles) using Kramers-like theory with the parameters of Table 5.

are strongly influenced by solvent tumbling. Despite larger λ values in acetonitrile by over 20% than those in benzonitrile, the rate constants are slightly smaller in the more viscous solvent for $\mathbf{3}^-$, and the Eyring plots in the two solvents cross in the range studied for $\mathbf{4}^-$. Quite good agreement with the experimental data is calculated using the parameters shown in Table 5.

Conclusion

The effects of solvent dynamics on the intramolecular ET reaction in the radical anions studied here increase in the order of $\mathbf{2}^- < \mathbf{4}^- < \mathbf{3}^-$, which corresponds to the order of how close these compounds lie to the Class II/Class III borderline, which is also the reverse order of their activation barriers. Solvent friction effects on rate constants are only detected for small energy barriers because otherwise, the exponential term dominates and the changes in activation energy mask the solvent effects on the pre-exponential factor. Unfortunately, in our case, faster reactions are inaccessible by ESR because for the nitrogen hyperfine constants normally found in dinitro-aromatic radical anions, the maximum limit for detection of linebroadening effects is $\sim 10^9 - 10^{10}$ s^{-1}. However, faster time scales can be reached by using infrared band broadening, as reviewed by Meyers et al.[28] and shown by Kubiak and co-workers for pyrazine-bridged mixed valence Ru clusters.[29]

Acknowledgment. We thank the National Science Foundation for support of this work under CHE-0647719 (S.F.N.), Fundação Para a Ciência e Tecnologia through its Centro de Química Estrutural (J.P.T.), and the National Science Foundation of China, 20773115, 20833004 (Y.Z.).

Supporting Information Available: ESR rate constants, hyperfine splittings, intrinsic line width parameters and Eyring plots for $\mathbf{2}^-$, $\mathbf{3}^-$, and $\mathbf{4}^-$ in all solvents studied, and τ values used for the fits in Figures 8 and 9. This material is available free of charge via the Internet at http://pubs.acs.org.

References and Notes

(1) (a) Ward, R. L. *J. Chem. Phys.* **1960**, *32*, 410. (b) Ward, R. L. *J. Am. Chem. Soc.* **1960**, *82*, 1296.

(2) See: Nelsen, S. F.; Weaver, M. N.; Konradsson, A. E.; Telo, J. P.; Clark, T. *J. Am. Chem. Soc.* **2004**, *126*, 15431–15438, refs 2−8 therein, and refs S1−S21 in its Supporting Information.

(3) (a) Robin, M.; Day, P. *Adv. Inorg. Radiochem.* **1967**, *10*, 247. (b) Hush, N. S. *Prog. Inorg. Chem.* **1967**, *8*, 391. (c) Hush, N. S. *Electrochim. Acta* **1968**, *13*, 1005.

(4) Mikhailov, M. N.; Medkovich, A. S.; Kuzminsky, M. B.; Ruskov, A. I. *J. Mol. Struct.: THEOCHEM* **2007**, *847*, 103–106.

(5) (a) Sutin, N. *Prog. Inorg. Chem.* **1983**, *30*, 441–99. (b) Marcus, R. A.; Sutin, N. *Biochim. Biophys. Acta* **1985**, *811*, 265–322.

(6) Nelsen, S. F.; Ismagilov, R. F.; Trieber, D. A., II. *Science* **1997**, *278*, 846–9.

(7) Nelsen, S. F. *Chem. Eur. J.* **2000**, *6*, 581–588.

(8) Demadis, K. D.; Hartshorn, C. M.; Meyer, T. J. *Chem. Rev.* **2001**, *101*, 2655–2685.

(9) Brunschwig, B. S.; Creutz, C.; Sutin, N. *Chem. Soc. Rev.* **2002**, *31*, 168–184.

(10) Nelsen, S. F.; Konradsson, A. E.; Weaver, M. N.; Telo, J. P. *J. Am. Chem. Soc.* **2003**, *125*, 12493–12501.

(11) Nelsen, S. F.; Weaver, M. N.; Telo, J. P.; Zink, J. I. *J. Am. Chem. Soc.* **2005**, *127*, 10611–10622.

(12) Heller, E. J. *Acc. Chem. Res.* **1981**, *14*, 368.

(13) Nelsen, S. F.; Weaver, M. N.; Telo, J. P. *J. Am. Chem. Soc.* **2007**, *129*, 7036–7043.

(14) Nelsen, S. F.; Schultz, K. P.; Telo, J. P. *J. Phys. Chem. A* **2008**, *112*, 12622–12628.

(15) Ruggli, P.; Lang, F. *Helv. Chim. Acta* **1938**, *21*, 38–50.

(16) Fraenkel, G. K. *J. Phys. Chem.* **1967**, *71*, 139–171; see eq 3.26, p 157.

(17) Rosokha, S. V.; Sun, D.-L.; Kochi, J. K. *J. Phys. Chem. A* **2002**, *106*, 2283–2292.

(18) (a) Lancaster, K.; Odom, S. A.; Jones, S. C.; Thayumanavan, S.; Marder, S. R.; Brédas, J. L.; Coropceanu, V.; Barlow, S. *J. Am. Chem. Soc.* **2009**, *131*, 1717–1723. (b) Barlow, S.; Risko, C.; Chung, S.-J.; Tucker, N. M.; Coropceanu, V.; Jones, S. C.; Levi, Z.; Brédas, J.-L.; Marder, S. R. *J. Am. Chem. Soc.* **2005**, *127*, 16900–16911.

(19) Nelsen, S. F.; Schultz, K. P. *J. Phys. Chem. A* **2009**, *113*, 5577–5584.

(20) Newton, M. D. *Chem. Rev.* **1991**, *91*, 767–792.

(21) (a) Gutmann, V. *Coord. Chem. Rev.* **1976**, *28*, 225–255. (b) Gutmann, V. *The Donor−Acceptor Approach to Molecular Interactions*; Plenum: New York, 1980.

(22) Nelsen, S. F.; Ismagilov, R. F.; Gentile, K. E.; Powell, D. R. *J. Am. Chem. Soc.* **1999**, *121*, 7108–7114.

(23) Horng, M. L.; Gardecki, J. A.; Papazyan, A.; Maroncelli, M. *J. Phys. Chem.* **1995**, *99*, 17311–17337.

(24) Zhao, Y.; Liang, W.-Z. *Phys. Rev. A* **2006**, *74*, 032706.

(25) Zhao, Y.; Liang, W.-Z.; Nakamura, H. *J. Phys. Chem. A* **2006**, *110*, 8204.

(26) Zhao, Y.; Milnikov, G. *Chem. Phys. Lett.* **2005**, *413*, 362.

(27) Grampp, G.; Jaenicke, W. *Ber. Bunsen-Ges. Phys. Chem.* **1991**, *95*, 904.

(28) Demadis, K. D.; Hartshorn, C. M.; Meyer, T. J. *Chem. Rev.* **2001**, *101*, 2655–2685.

(29) (a) Lear, B. J.; Glover, S. D.; Salsman, J. C.; Londergan, C. H.; Kubiak, C. P. *J. Am. Chem. Soc.* **2007**, *129*, 12772–12779. (b) Salsman, J. C.; Kubiak, C. P.; Ito, T. *J. Am. Chem. Soc.* **2005**, *127*, 2382–2383. (c) Londergan, C. H.; Kubiak, C. P. *Chem.—Eur. J.* **2003**, *9*, 5962–5969. (d) Ito, T.; Hamaguchi, T.; Nagino, H.; Yamaguchi, T.; Kido, H.; Zavarine, I. S.; Richmond, T.; Washington, J.; Kubiak, C. P. *J. Am. Chem. Soc.* **1999**, *121*, 4625–4632. (e) Ito, T.; Hamaguchi, T.; Nagino, H.; Yamaguchi, T.; Washington, J.; Kubiak, C. P. *Science* **1997**, *277*, 660–663.

JP9017508